Investigation on laser absorption and x-ray radiation in microstructured titanium targets heated by short-pulse relativistic laser pulses

X. Pan,[1,2,*] M. Šmíd,[1] L. G. Huang,[1] T. Kluge,[1] V. Bagnoud,[3,4] E. Brambrink,[5] T. E. Cowan,[1,2] J. Colgan,[6] T. Ebert,[7,8] D. Hartnagel,[7] M. Hesse,[7] J. Hornung,[4] A. Kleinschmidt,[4] P. Perez-Martin,[1,2] A. Neukirch,[6] K. Philipp,[2] S. Sander,[7] G. Schaumann,[7] A. Tebartz,[7] B. Zielbauer,[4] M. Roth,[7] and K. Falk[1,2,9]

[1]*Institute of Radiation Physics, Helmholtz-Zentrum Dresden-Rossendorf, 01328 Dresden, Germany*
[2]*Faculty of Physics, Technische Universität Dresden, 01069 Dresden, Germany*
[3]*Institut für angewandte Physik, Technische Universität Darmstadt, 64289 Darmstadt, Germany*
[4]*Plasmaphysik, GSI Helmholtzzentrum für Schwerionenforschung, 64291 Darmstadt, Germany*
[5]*Laser Group, European XFEL, Holzkoppel 4, 22869 Schenefeld, Germany*
[6]*Theoretical Division, Los Alamos National Laboratory, Los Alamos, New Mexico 87545, USA*
[7]*Institut für Kernphysik, Technische Universität Darmstadt, 64289 Darmstadt, Germany*
[8]*X-ray Measurement and Diagnostic Science, Lawrence Livermore National Laboratory, Livermore, California 94550, USA*
[9]*PALS Centre, Institute of Physics of the ASCR, 18221 Prague, Czech Republic*

(Received 19 April 2023; accepted 29 November 2023; published 8 January 2024)

The enhancement effect of a microstructured surface on laser absorption and characteristic Kα emission has been investigated by measuring K-shell emission from titanium (Ti) targets irradiated with high-intensity ($\sim 10^{20}$ W cm^{-2}), subpicosecond (500 fs) laser pulses. The experimental results indicate a modest enhancement (1.6×) of Kα emission from microstructured targets compared to flat foils, but with a similar intensity and profile of Heα and Li-like satellites. Particle-in-cell (PIC) simulations are implemented to further understand the underlying physical processes in the laser interaction with both targets, interpreting the mechanisms responsible for the Kα enhancement. The reasons for the lower-than-expected enhancement of Kα emission are discussed. The rapid heating of the bulk plasma might result in the premature shutdown of Kα emission before the thermalization of hot electrons or even the end of laser pulses, suggesting that the use of Kα emission as a diagnostic of the hot-electron yield or relaxation could lead to a misinterpretation.

DOI: 10.1103/PhysRevResearch.6.013025

I. INTRODUCTION

The high-intensity, short-pulse laser irradiation of solid targets can create extremely high temperature, near-solid density plasmas, not only providing a unique platform for the study of high energy density (HED) physics but also serving as compact, short-duration radiation and energetic particle sources [1–6]. In particular, the production of high peak-brightness ultrashort x-ray sources with laser pulses is of tremendous interest for probing ultrafast real-time dynamics in physical and chemical systems, and biomedical imaging [7–15]. It has been demonstrated that laser-produced x-ray sources can provide sufficient photon numbers in narrow-band spectral lines to perform spectrally resolved x-ray Thomson scattering (XRTS) measurements in dense plasmas [9–13], which can provide important physical properties including temperature, density, ionization state, and microscopic structure. In addition, laser-driven x-ray sources are also widely used as high-brightness backlighters for radiography in the inertial confinement fusion (ICF) and other HED experiments [14,15].

It is crucial and desired to develop a laser-driven x-ray source with a higher brightness, especially for applications that require a very high photon flux in a narrow spectral bandwidth, e.g., XRTS. One key to enhancing x-ray radiation is improving the laser energy absorption by the target. However, the laser-to-target coupling is usually limited due to the reflection of the incident laser caused by the critical electron density in the surface plasma [16]. In order to enhance the laser-to-target coupling and thus the brightness of laser-driven x-ray sources, various techniques have been employed. An increase in Kα yield per laser energy can be observed with increasing the laser intensity up to $\sim 10^{18}$ W/cm^2, and thereafter the conversion efficiency of laser energy to Kα emission is approximately constant [14]. High contrast lasers can also improve Kα and bremsstrahlung yields by suppressing the preplasma formation [17,18]. Another approach is optimizing the morphology of targets. The enhancements in laser absorption and x-ray radiation have been observed experimentally by using structured targets [19–26], subwavelength grating targets [27,28], or foams [29]. More recently, a novel microstructured target made of silicon (Si) has been investigated, demonstrating a significant increase (12×) of Kα emission [30]. Structured targets can substantially diminish the reflection of laser energy, enhance local electric fields [24,27], and

*panxy@hzdr.de

promote the vacuum heating process [25,30], thus improving laser absorption and x-ray radiation. The vacuum heating in microstructured targets arises mainly from sharp plasma-vacuum interfaces formed on the sloping microsurfaces [31]. The main advantage of microstructured targets compared to nanostructured targets is that the durability of the structures during the laser-solid interaction can be improved. For applications that require a narrow spectral bandwidth source, e.g., XRTS experiments, a cold Kα source is preferred over thermal Heα or Lyα sources and hard x-ray bremsstrahlung sources due to the absence of prominent satellite lines in Kα emission. Moreover, laser-driven Kα emission has a much shorter duration and smaller source size compared to thermal spectral lines and bremsstrahlung emission, resulting in a better temporal and spatial resolution of the probing. However, the Kα yield is usually much lower than Heα and Lyα yields [12], as well as the overall bremsstrahlung yield. Up to now, most laser-driven x-ray sources used for XRTS measurements are still based on Heα or Lyα emission [9–13]. The XRTS measurement for shock-compressed carbon foam using a laser-produced titanium (Ti) Kα source has been preliminarily demonstrated, but still with a weak scattering signal [32]. Thus, further enhancing laser-driven Kα sources is of paramount importance for dense plasma experiments.

Laser energy absorption is a complex physical process where hot (or fast) electrons play a vital role in transferring the laser energy into the target. In a relativistic laser-solid interaction ($I\lambda^2 > 1.3 \times 10^{18}$ W μm/cm^2), electrons are accelerated to relativistic energies mainly by the pondermotive force, resulting in a Maxwellian-like temperature distribution [33,34]. For short-pulse lasers with moderately intense but nonrelativistic intensities (10^{15} W/cm^2 $< I < 10^{18}$ W/cm^2), hot electrons are produced basically by two other collisionless absorption mechanisms, i.e., resonance absorption and vacuum heating [31,34,35]. Bulk plasmas can be heated to hundreds of eV and even several keV by hot electrons via the cold return current and direct collision mechanisms [36,37]. Although the electrons with energies above the plasma sheath potential will leave the backside of the target, hot electrons with relatively low energies can deposit their energies inside the target through the single-pass or refluxing processes [38,39]. Meanwhile, various x-ray emission lines are generated in the plasma, including the characteristic Kα emission produced via K-shell ionization caused by hot electrons [40]. The conversion efficiency of laser energy to x-ray radiation depends on the hot electron production, which is determined by the conditions of the laser-target interaction. K-shell emission measurements have been widely used as the reliable spectroscopic diagnostics for dense plasmas [41–45], because the atomic levels involved in K-shell emission are sensitive to the plasma conditions.

In this paper, we present K-shell emission measurements for both flat and microstructured Ti targets irradiated by a high-intensity, short-pulse laser, to investigate the effect of microstructures on laser absorption and characteristic x-ray emission. The experimental results are complemented with particle-in-cell (PIC) simulations to interpret the underlying physics in the laser interaction with both targets. Section II describes the experimental setup. The experimental results and analysis are presented in Sec. III. Section IV gives the discussion on the limited enhancement of Kα emission. The article is concluded in Sec. V.

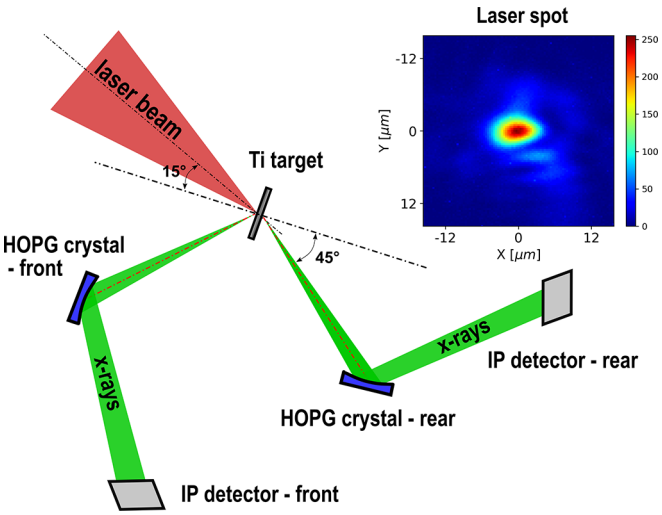

FIG. 1. Schematic of the experimental setup (not to scale) and measured laser focal spot.

II. EXPERIMENTAL SETUP

The experiment was conducted at the PHELIX laser facility [46] at the GSI Helmholtzzentrum für Schwerionenforschung in Darmstadt, Germany. Figure 1 shows the schematic of the experimental setup. The *s*-polarized laser beam with an average energy of ∼100 J and a pulse duration of 500 fs was delivered to the target at the fundamental wavelength of 1053 nm. The laser was focused by a copper off-axis parabolic mirror to a focal spot of ∼8 μm full width half maximum (FWHM) at an incident angle of ∼15° relative to the target normal. Approximately 35% of the laser energy was estimated to be contained in the 8 μm diameter spot, thus a mean peak intensity of $\sim 1.4 \times 10^{20}$ W cm^{-2} was obtained on the target. The temporal contrast of the laser pulse was measured to be $\sim 10^{10}$ at 150 ps before the peak intensity [47,48], which can significantly suppress the long-scale preplasma and thus reduce the back reflection of laser energy [16].

Two cylindrically curved highly ordered pyrolytic graphite (HOPG) [49,50] crystal spectrometers were employed to observe the K-shell emission of Ti targets from the front and rear sides, respectively, as illustrated in Fig. 1. Both spectrometers were in Von Hamos geometry and had identical geometrical configurations. The HOPG crystals used had a mosaic spread of $m = 0.8°$, a thickness of 30 μm and a lattice spacing of $2d_{002} = 6.708$ Å. The size of each crystal was 40 mm × 20 mm and the radius of curvature was 115 mm. The two crystals were placed 300 mm from the target at the front and rear sides, respectively, and centered at $E = 4510$ eV (Bragg angle $\theta_B = 24.2°$). The x-ray spectra were detected by the FujiFilm BAS-TR image plates (IPs), which were placed 300 mm from their corresponding crystals with the orientation perpendicular to the reflected beam from the crystal. Pokalon foils were put in front of the IPs as light-tight filters. In addition, 10–30 μm thick aluminum foils were also placed in

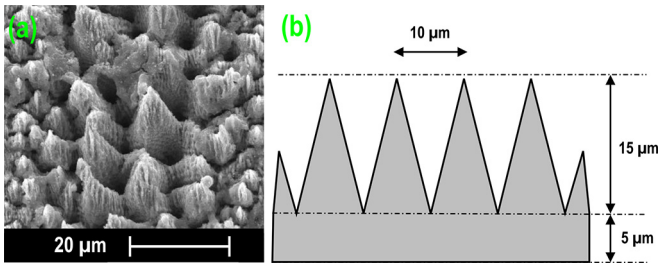

FIG. 2. The (a) SEM image and (b) schematic cross section of microstructured titanium targets.

front of the IPs as the x-ray filter to avoid saturation of Kα or Heα signal on the detector.

Two types of Ti targets were used, namely flat targets and microstructured targets. The flat targets were 10 μm thick polished Ti foils. The microstructured targets were Ti substrates with conical microstructures on one side. These conical microstructures were fabricated by irradiating Ti samples with a train of ultrashort (∼100 fs) laser pulses [51], resulting in a height of 15 μm and a base width of 10 μm. The remaining substrate thickness was approximately 5 μm. The scanning electron microscope (SEM) image and schematic of the microstructured Ti targets are shown in Fig. 2. These microstructures (front side) were facing the laser beam during the experiment. The enhancement effect of the microstructures on laser absorption and x-ray radiation was benchmarked by the 10 μm thick flat targets.

III. RESULTS AND ANALYSIS

Time-integrated K-shell emission spectra were measured for the two types of Ti targets and laser energies varying from 80 to 110 J. The typical K-shell emission spectra measured are shown in Fig. 3, in which the spectra recorded from the rear and front sides of the target are denoted as the rear spec and front spec, respectively. The spectral intensity has been converted into the unit of photostimulated luminescence (PSL) [52], and corrected for the transmission of x-ray filters. Because the IPs were scanned at the same time after each shot, no correction for IP fading is needed for the spectral comparison. Multiple distinct emission lines, including the "cold" Kα line and thermal lines (i.e., Heα and its Li-like satellites), are observed from both sides of the target. Kα lines are prominent in both front and rear spectra, and have almost the same intensity and line shape. By contrast, thermal lines are dominant in the front spec, but are much weaker in the rear spec.

The different ratios of Heα to Kα in both spectrometers can be explained due to radiation transport effects. The Kα emission is driven mostly by the hot electrons, which are distributed close to homogeneously along the target depth. Also, the absorption of Ti foil is relatively small for its energy, around 40% for the whole 10 μm thickness, therefore the close-to-isotropic emission of Kα is expected. On the other hand, the Heα and Li-like radiation are mostly formed in the hot plasma on the front surface of the target. Though the absorption of those lines in cold Ti is very low, it is rapidly increasing with plasma temperature up to approximately 1 keV. For example, according to the collisional-radiative model FLYCHK [53], the absorption in a 400 eV hot, 10 μm thick solid-density Ti plasma is well above 90% over the range 4600–4750 eV. In addition to the radiation transport effects, the different ratios of Heα to Kα in both spectrometers might also be affected by different crystal reflectivities over the measured spectral range.

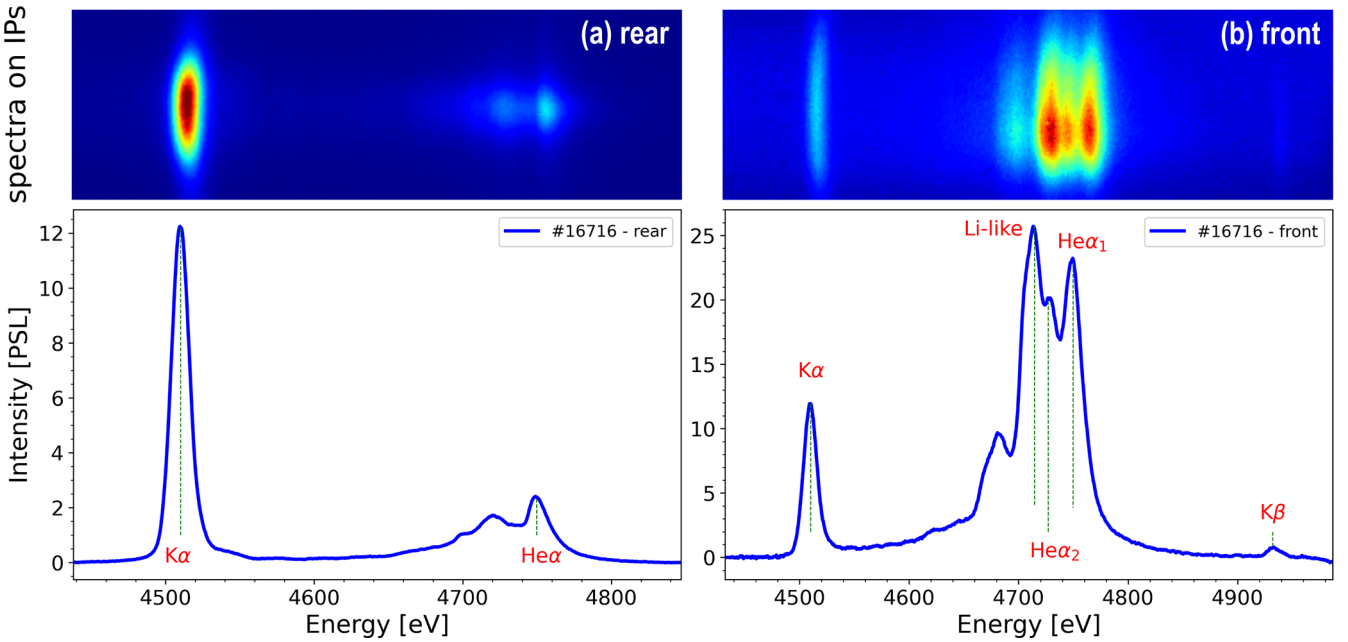

FIG. 3. Single-pulse K-shell emission spectra measured by two HOPG spectrometers. The spectra recorded from the (a) rear and (b) front sides of the target are denoted as rear spec and front spec, respectively. Note that the two plots have different energy and intensity ranges and color bars.

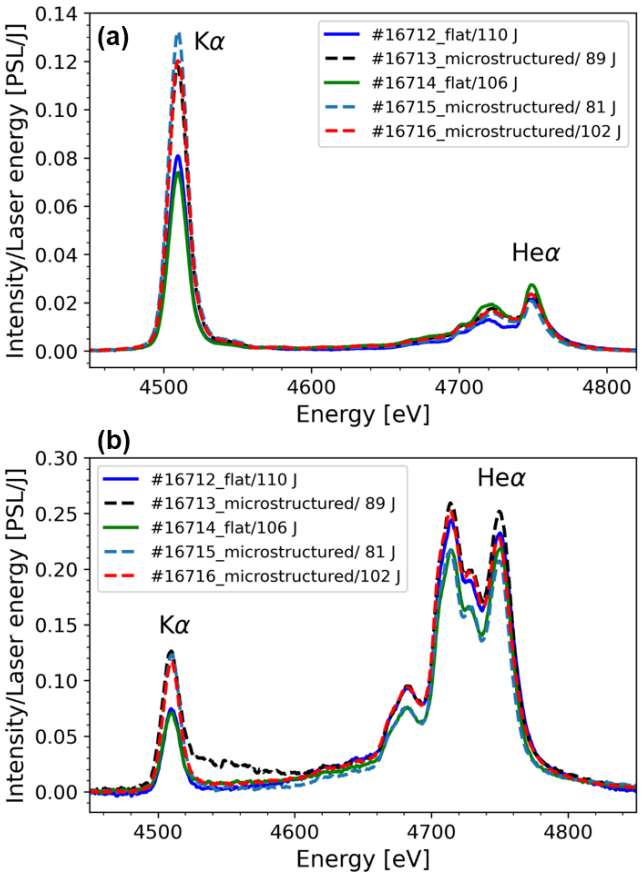

FIG. 4. Comparison of K-shell spectra at different experimental conditions from the (a) rear and (b) front spectrometers.

The K-shell emission spectra from different targets and laser energies are compared in Fig. 4, showing an obvious enhancement of Kα emission in microstructured Ti targets. The spectral intensity has been normalized by the laser energy to remove its influence on the radiation yield [14,54]. The relative Kα yield is estimated by the integral of the normalized spectral intensity within the interval of 4490–4530 eV. There is a $\sim$1.6$\times$ increase of Kα yield in microstructured targets compared to flat foils, indicating a modest enhancement of the hot electron production and laser energy absorption. The Heα yield and line shape in flat and microstructured targets are comparable, implying that the microstructures do not enhance the overall achieved plasma temperature. To better understand the underlying processes of the laser interaction with flat and microstructured targets, a series of PIC simulations including the collision and ionization effects (field and direct impact) were performed with the PICLS code [55]. Due to the dramatically increased numerical heating in the late phase of two-dimensional (2D) real-density simulations, 2D reduced-density simulations were chosen for comparing the heating processes in flat and microstructured targets. Meanwhile, a one-dimensional (1D) real-density simulation gave a reasonable evaluation of real plasma conditions, and was consequently used as a benchmark for 2D reduced-density simulations. The 2D PIC simulations were implemented in a 2D3V geometry for Ti targets with a reduced ion density of 4 n_c, corresponding to 88 n_c free electron density in a fully ionized case, where $n_c = 1.0 \times 10^{21}\,\mathrm{cm}^{-3}$ was the plasma critical density for the laser wavelength $\lambda_0 = 1053$ nm. The target material was preionized with the charge state of 20 and initialized with 0 eV temperature and 5 Ti^{20+} ions per cell. The laser pulse was modeled by a Gaussian spatial profile with an FWHM spot size of 8 μm, a sinusoidal temporal profile with an FWHM duration of 500 fs, and a peak intensity of $I_0 = 1.24 \times 10^{20}\,\mathrm{W/cm^2}$, corresponding to a normalized vector potential of $a_0 = 0.85\lambda_0[\mu\mathrm{m}](I_0[\mathrm{W/cm^2}]/10^{18})^{1/2} = 10$. This temporal profile was chosen to shorten the simulation time for the early rising edge while maintaining a similar laser main pulse shape with the Gaussian profile. The prepulse was neglected in the simulations, which is acceptable for such a high-contrast laser. The incidence angle of the laser was set to two values, i.e., 0° and 15°, to investigate the impact of the incidence angle on the target heating. The simulation box size was $30 \times 60\,\mu\mathrm{m}^2$ with a spatial grid resolution of 17 nm and absorbing boundaries. In addition, the 1D PIC simulation was implemented in a 1D3V geometry for the Ti target with a real solid density of 56 n_c, a preionization of two, and a thickness of 10 μm. The laser pulse had the same intensity as in the 2D simulations but with a Gaussian temporal profile (500 fs FWHM duration), and propagated along the spatial dimension of the target thickness direction.

The bulk electron temperatures (T_e) from 2D reduced-density simulations are corrected by a scaling factor of 0.41, which is gained from the comparison with the results of the 1D real-density simulation, as shown in Fig. 5. The 2D simulations start at −500 fs, and 0 fs corresponds to the moment of the peak intensity arrival on the target surface. The simulations for 15° incidence have similar results, not detailed here. Compared to the flat target, the microstructured target demonstrates an increased interaction surface, spiky features signifying vacuum heating [31], and comparable electron temperature. The exposed surface area of the microstructured target is multiple times larger than that of the flat foil, thus more electrons are heated in the microstructured target during the laser-matter interaction, which can be seen in the electron energy spectrum (EES) shown in Fig. 6. The larger interaction surface also results in a reduced laser intensity, of which the effect on the temperature is partially compensated by the additional vacuum heating in the microstructured target. Vacuum heating [31], also known as the Brunel effect, is a collisionless absorption mechanism in which the electric field of the incident laser drives the electron oscillations across the plasma-vacuum interface. It occurs when an intense laser field is incident obliquely on a sharply bounded overdense plasma. In this case, the excursion of electrons at the plasma-vacuum interface is so large that the electrons can be literally dragged into the vacuum and then sent back into the plasma [35]. As demonstrated by Fig. 5(b), the vacuum heating occurs in the early phase of laser interaction with the microstructured target due to its sloping surface, then vanishes as the density gradient at the vacuum-target boundary diminishes. It is worth mentioning that the impact of vacuum heating will be reduced in the plasma with a real preplasma gradient. Nonetheless, with the existence of an under -dense preplasma, other heating mechanisms, e.g., resonance absorption, might also exist in the microstructured targets.

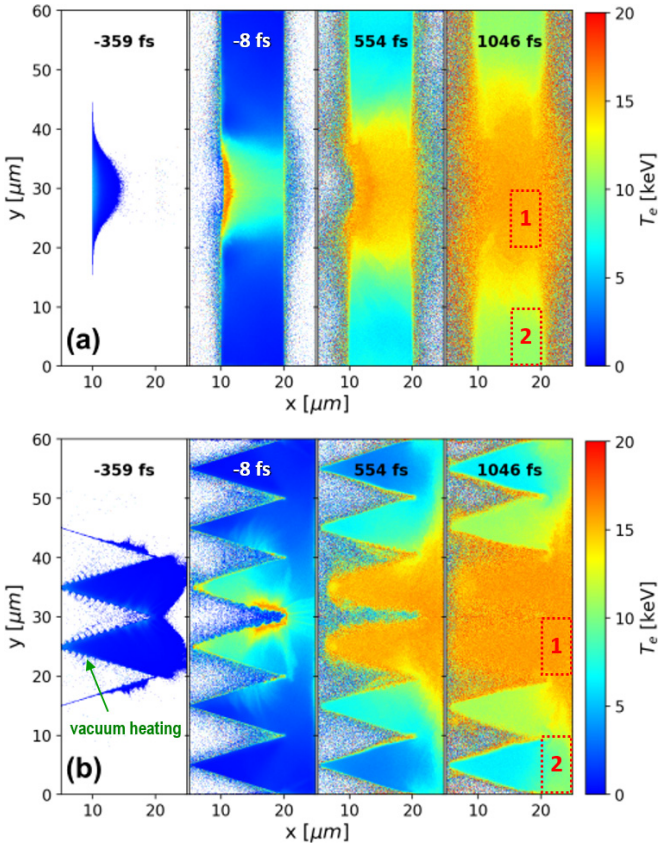

FIG. 5. Bulk electron temperatures (T_e) of different times in (a) flat and (b) microstructured Ti targets obtained from 2D reduced-density PIC simulations at 0° laser incidence. Only the x range of 5 to 25 μm are shown in the plots. In plot (b), the little "spikes" on the slopes of the microstructured target are the signature of vacuum heating. Red dashed boxes marked by 1 and 2 represent the central (near y=30 μm) and edge (near y=0 μm) regions of the targets, respectively.

Additionally, more laser light gets trapped in the conical microstructures because the reflected light will interact with the opposite surfaces as well. Therefore, the amount of directly back-reflected light is reduced and the overall absorbed laser energy is increased. PIC simulations indicate that the laser absorption is enhanced by ∼80% in microstructured targets compared to flat targets. In a similar experiment by Ebert *et al.* [30], using Si structures with similar scale and shape, the reflected fundamental light and second harmonic emission were reduced by ∼70% and ∼90%, respectively, in microstructured targets compared to flat foils. This experimental result is in good agreement with our simulations. Another advantage of these structures is that they can trap the plasma, thereby increasing the interaction volume [56]. The combination of vacuum heating and geometric trapping effect counteracts the effect of the decreased laser intensity on microstructured targets, resulting in a comparable electron temperature with flat foils.

The detailed electron heating processes are shown by the temporal evolution of the EES in Fig. 6. For further discussion, we define three groups of electrons. The first one, with kinetic energies below 100 keV, is called thermal electrons, as they follow the Maxwellian distribution. Second, the electrons with kinetic energies of several hundred keV are named moderate electrons. Finally, the most energetic electrons with kinetic energies above 1 MeV are referred to as high energy electrons. In the initial interaction phase, a larger number of electrons, including thermal electrons and high energy electrons, are heated or accelerated by the laser in microstructured targets compared to flat targets, and the cut-off energy of electrons in microstructured targets is higher as well. This phenomenon can be explained by the enlarged surface and additional vacuum heating of microstructured targets, as illustrated before. Along with the laser irradiation, more high energy electrons are generated and then accelerated to the maximum energy approximately at the arrival of laser peak intensity. In this process, high energy electrons transfer the energy to bulk electrons via return current or direct collisions [36], resulting in the rise of bulk electron temperature. This is demonstrated by the increased number of the high-energy tail of thermal electrons in Fig. 6. Once the laser pulse is over, the thermalization of high energy electrons continues by transferring their energy to bulk electrons. During the whole simulation, the microstructured target always has more high energy electrons and higher "hot-electron temperature" ($T_{\rm hot}$) than the flat target, explaining the enhancement of Kα emission in the microstructured target. The $T_{\rm hot}$ is a quantitative description of the hot-electron energy distribution, estimated by an exponential fit to the slope of the high energy electron spectrum, which is possible due to its Maxwellian-like distribution [36,57]. The incidence angle has a slight impact on the electron heating. A larger number of hot electrons, but with a lower $T_{\rm hot}$, is observed in the 0° incidence simulations than 15° incidence simulations. This results in slightly different energy distributions for high energy electrons.

IV. DISCUSSION

The laser coupling to the target is improved significantly in microstructured targets compared to flat foils, as demonstrated by PIC simulations. However, the enhancement of Kα emission is not as significant as in the previous study using similar microstructured Si targets under comparable conditions [30]. Interestingly, earlier studies, which use nano or microstructured targets for increasing laser energy absorption, demonstrate at least one order of magnitude of enhancements of x-ray bremsstrahlung, but only modest enhancements (<2×) of Kα emission [21–27]. A decreased intensity of Kα emission is even observed in the nanostructured ZnO target while the laser absorption is enhanced twofold [58]. Although laser parameters and target morphologies are various in these studies, we can still conclude that, in contrast to bremsstrahlung radiation, Kα emission is less sensitive to the target morphology. These research results, together with our experimental results, present a question of why the enhancement of Kα emission is not significant in many structured targets while the laser absorption is enhanced substantially.

Our study provides a plausible explanation for this phenomenon. While previous studies have primarily linked the x-ray emission with the enhanced laser absorption, Kα emission is directly subjected to the K-shell ionization arising

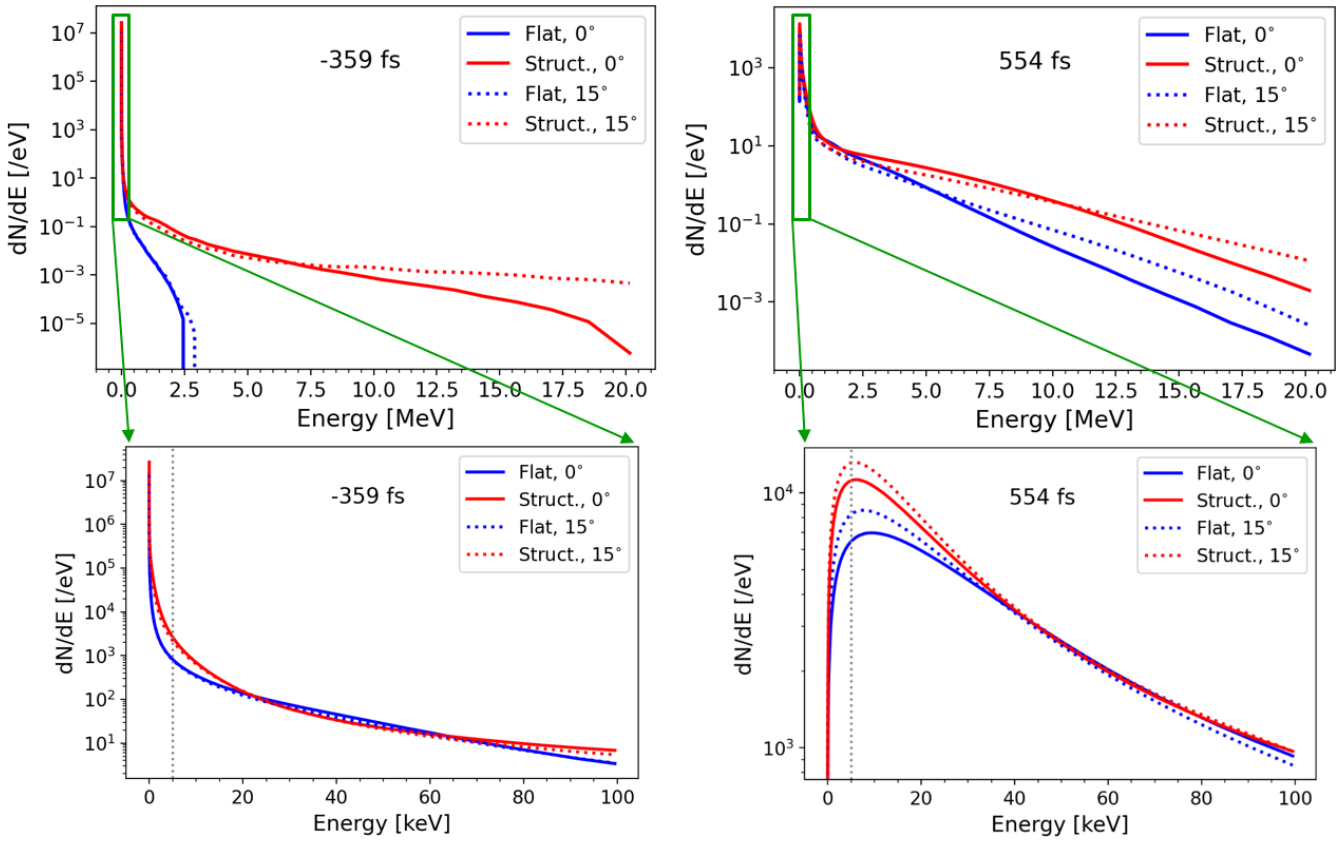

FIG. 6. Electron energy spectrum (EES) at different times extracted from PIC simulations. The bottom row shows the zoom ins of the EES from the green rectangles above, showing the range of 0 to 100 keV to compare the thermal electron populations in different targets. Solid and dotted curves represent 0° and 15° laser incidences, respectively. The vertical dashed lines denote the 5 keV electron energy threshold.

from the impact of hot electrons on cold materials. The first obvious explanation could be the limited enhancement of hot electron numbers in structured targets. Our PIC simulations show only a modest enhancement (∼1.3×) of the number of electrons with energies above the Ti K-shell electron binding energy (∼5 keV) in the microstructured target. The quantitative comparison of absolute numbers of free electrons in our PIC simulations is, however, unreliable due to artificial factors (e.g., reduced density). We thus refer to other experiments with similar target structures and comparable laser conditions that show a clear enhancement in the hot electron numbers and thus we expect a similar trend in our study [30]. Unfortunately, no reliable electron diagnostics that would measure both the escaping electrons and those generated within the targets and trapped there were available during this experiment to obtain the actual numbers of hot electrons generated in two types of targets, such as Faraday cup, Thomson parabola spectrometer, bremsstrahlung, or Cherenkov detectors [59–62]. Additionally, compared to 10 μm thick flat foils, the thinner (5 μm) substrate of microstructured targets reduces the available deposited energy of escaping hot electrons for K-shell ionization in the cold volume.

An alternative explanation is presented here, where the rapid heating of bulk targets might also constrain the production of Kα photons. To verify this hypothesis, the temporal evolution of scaled bulk electron temperatures (T_e) in two different target regions (central and edge), illustrated in Fig. 5, are extracted from the reduced-density PIC simulations and shown in Fig. 7. These two regions are selected to represent the inhomogeneous heating of the target bulk. In both regions, the T_e rises rapidly as the laser irradiates the target, and the heating process in microstructured targets is significantly faster than that in flat targets. According to the spectral modeling using the collisional-radiative SCFLY code [41], once T_e is over 100 eV, the Ti L-shell electrons start to be ionized resulting in the emission of blue-shifted L-shell satellites while the "cold" Kα emission disappears. It is important to note that the collisional cross section for K-shell ionization is significantly decreasing as the plasma temperature (or charge state) increases [63], these intermediate shifted L-shell satellites are thus very weak and not observed in our measured spectra. Therefore, 100 eV is taken as the upper threshold of T_e for generating "cold" Kα emission in Ti targets. Figure 7 indicates that T_e in the central and edge regions of the microstructured target reach 100 eV at −310 fs and −140 fs, respectively. The time window (t_{win}) for generating "cold" Kα emission is thus very short (a few hundred fs timescale), occurring prior to the arrival of the peak intensity on the target. Due to the faster heating process, microstructured targets have an even shorter time window of "cold" Kα emission compared to flat targets. This factor sort of counteracts the effect of more hot electrons in microstructured targets. Thus, the increased production of hot electrons cannot be effectively converted into the increase of Kα yield. While our simulations predict

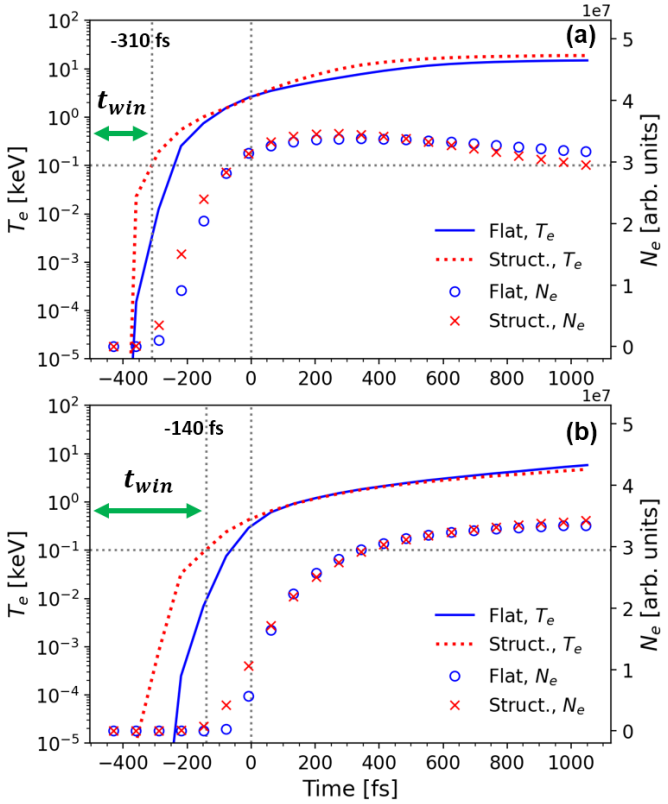

FIG. 7. Temporal evolution of bulk electron temperatures (T_e) and above 5 keV electron number (N_e) in the (a) central and (b) edge regions (as marked by boxes 1 and 2 in Fig. 5). $T_e = 100$ eV is denoted by the horizontal dotted lines. The $t_{\rm win}$ refers to the time window of "cold" Kα emission.

the peak bulk temperature around 15 keV, past experimental work confirms that keV level temperatures are reached at the given laser conditions [64,65]. It is expected that the PIC simulation is likely to overestimate the bulk temperature, however the above conclusion still holds with downscaling the temperature even by one order of magnitude.

To further investigate the dynamic process of Kα production, the temporal evolution of the electron numbers in different energy ranges is plotted, see Fig. 8. These electrons are chosen from the whole PIC simulation box and with kinetic energies above 5 keV. As shown in Fig. 8, the evolution trends of electron numbers are comparable for 0° and 15° laser incidences and overlap completely within $t_{\rm win}$. Compared to flat targets, a clearly increased number of thermal electrons above 5 keV as well as high energy electrons is generated in microstructured targets as the laser irradiates. This increased electron number accounts for the enhancement of Kα emission in microstructured targets. However, this effect stops when the bulk electron temperature rises up to the upper threshold temperature of Kα emission. The following increase of this electron number does not contribute to the Kα radiation, but still generates more x-ray bremsstrahlung, which explains the different enhancements of Kα and hard x-ray emission in structured targets [24,26]. Therefore, the rapid heating of bulk materials could be the major reason for modest enhancements of Kα emission in many structured targets. The number of moderate electrons is almost the same in both flat and microstructured targets during the initial interaction phase, then tends to diverge due to the thermalization of high energy electrons. Thus, moderate electrons can generate Kα photons, but do not contribute to the difference of Kα yields in both target morphologies.

In addition, high-energy thermal electrons contribute the most to the production of Kα emission because of (i) their dominant number within the electrons above 5 keV and (ii) the larger K-shell ionization cross sections of Ti in the electron energy range of several tens keV [66]. This dominant effect of high-energy thermal electrons on Kα emission is also observed in another experiment by Sander *et al.* [67], in which Cu Kα emission is decreased by ∼70% in a "flat Si + Cu" target where electrons with energies below 38 keV are stopped in the 15 μm Si front layer. As for the significant increase (12×) of Kα emission in the microstructured Si targets [30], it could occur due to the K-shell electron binding energy of Si being much lower (∼1.84 keV), thus more thermal electrons can contribute to the Kα emission before the onset of a high bulk temperature. Moreover, the microstructured Si targets have a more "spiky" geometry with a higher aspect ratio and can therefore better trap the light and plasma.

In fact, measurements of absolute Kα radiation intensity are commonly used to estimate the number of hot electrons generated during the complex laser-target interaction [57]. Our research result suggests that using Kα emission to

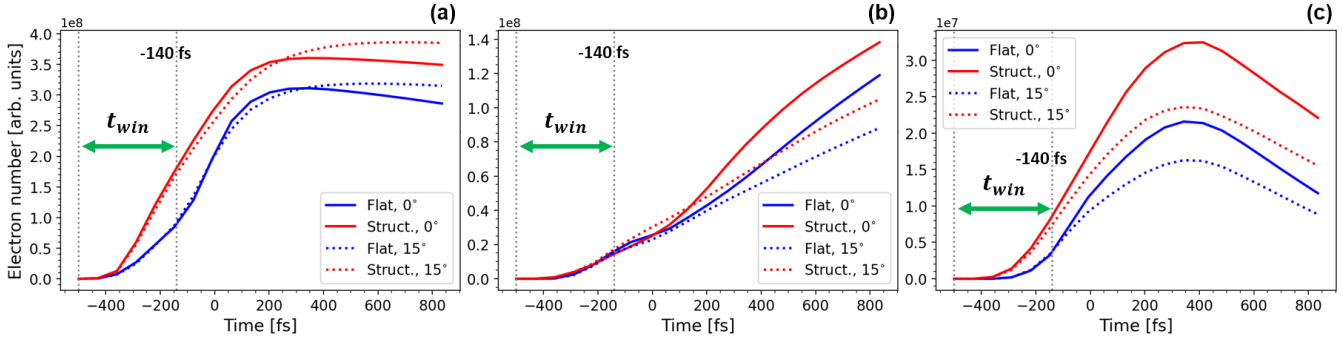

FIG. 8. Temporal evolution of all electron numbers in the energy ranges of (a) 5–100 keV (i.e., high-energy thermal electrons), (b) 100 keV–1 MeV (i.e., moderate electrons), and (c) >1 MeV (i.e., high energy electrons). The $t_{\rm win}$ corresponds to the time window of Kα production in the edge region of the microstructured target. Solid and dotted curves represent 0° and 15° laser incidences, respectively.

diagnose the hot electron production or relaxation time could lead to a misinterpretation, especially for sub-ps to ps high-power lasers compared to the tens of fs lasers. First, Kα photons can be produced by not only nonthermal electrons, but also the high-energy tail of thermal electrons. Second, the rapid heating of the bulk target could shut down the Kα emission before the end of the hot electron generation or thermalization. Because of the above reasons, care must be taken when using Kα yields to estimate the coupling efficiency of laser to the target or using time-resolved Kα spectroscopy to study hot electron relaxation processes for the high-power laser-solid interaction experiments, e.g., fast ignition (FI).

Several schemes can be adopted to improve the conversion efficiency of laser energy to Kα radiation for quasimonochromatic probing applications. For example, the size and geometry of the microstructures could be optimized to further enhance laser absorption and hot electron production. The substrate thickness of the structured targets could be optimized as well to maximize the Kα yield by considering both the generation and reabsorption of Kα photons in cold materials. Most importantly, the premature heating of bulk materials should be avoided or suppressed. This can be realized by using two-layer targets with a metal layer on the back side emitting the characteristic Kα lines. The front layer, made of other materials (e.g., C, Si), prevents direct illumination of the metal back layer, thus eliminating any direct laser heating. No substantial heating occurs in the back layer during the laser pulse [57]. The front layer can be structured targets as well for enhancing the laser absorption. A two-layer "microstructured Si + Cu" target was investigated under similar conditions at the PHELIX laser system, demonstrating an enhanced, clean Cu Kα source with the thermal emission suppressed significantly [67]. A thin front layer of lighter materials is preferred, because more electrons can pass through the front layer and contribute to the K-shell ionization of the back material.

V. CONCLUSIONS

The effect of microstructure morphology on laser energy absorption and characteristic x-ray radiation was studied by measuring K-shell emission from the flat and microstructured Ti targets irradiated by short-pulse, relativistic laser pulses. $\sim$1.6$\times$ increase of Kα emission was observed in microstructured targets compared to flat foils, indicating an enhancement of the laser energy absorption. The similar Heα and Li-like satellites between flat and microstructured targets implied a comparable bulk electron temperature in both targets. A series of PIC simulations were performed to further understand the underlying physical processes, demonstrating the increases of electron numbers and energies in microstructured targets as well as the enhanced laser absorption ($\sim$1.8$\times$). The enhancement effect was attributed to the increased interaction surface, additional heating mechanisms (e.g., vacuum heating), and geometric trapping of light in microstructured targets. Compared to the other experiment observing 12$\times$ enhanced Kα yield using structured Si targets [30], the reasons for the lower-than-expected enhancement of Kα emission in many structured targets were also discussed in detail. In particular, the premature shutdown of Kα emission caused by the rapid heating of bulk targets might be the major reason. The discussion also reveals the importance of *in situ* electron diagnostics that could measure the actual numbers of hot electrons generated in the targets for these experiments.

This rapid heating, which causes the premature shutdown of Kα emission, could strongly affect the accuracy of the Kα diagnostics and even lead to a misinterpretation of the hot electron production and relaxation processes. The premature heating of bulk materials could be prevented by using a two-layer target. With an optimized structured front layer, the high-brightness laser-produced Kα sources are promising for quasimonochromatic probing applications in high energy density physics and other fields, but this needs to be further explored.

ACKNOWLEDGMENTS

We acknowledge the whole PHELIX team at GSI for provision of high-power laser beamtime and their assistance during the experimental campaign. We would also like to thank the HZDR technical staff for machining the components of the spectrometers. This work is funded by the Helmholtz Association under Grant No. VH-NG-1338 and Laserlab Europe Proposal No. GSI002404. The work of J. Colgan and A. Neukirch was supported in part by the US Department of Energy through the Los Alamos National Laboratory. Los Alamos National Laboratory is operated by Triad National Security, LLC, for the National Nuclear Security Administration of U.S. Department of Energy (Contract No. 89233218CNA000001).

[1] R. P. Drake, *High-Energy-Density Physics: Fundamentals, Inertial Fusion, and Experimental Astrophysics* (Springer Berlin Heidelberg, 2006).

[2] G. A. Mourou, T. Tajima, and S. V. Bulanov, Optics in the relativistic regime, Rev. Mod. Phys. **78**, 309 (2006).

[3] J. D. Kmetec, C. L. Gordon, J. J. Macklin, B. E. Lemoff, G. S. Brown, and S. E. Harris, Mev x-ray generation with a femtosecond laser, Phys. Rev. Lett. **68**, 1527 (1992).

[4] C. Reich, P. Gibbon, I. Uschmann, and E. Förster, Yield optimization and time structure of femtosecond laser plasma *K*α sources, Phys. Rev. Lett. **84**, 4846 (2000).

[5] R. A. Snavely, M. H. Key, S. P. Hatchett, T. E. Cowan, M. Roth, T. W. Phillips, M. A. Stoyer, E. A. Henry, T. C. Sangster, M. S. Singh *et al.*, Intense high-energy proton beams from petawatt-laser irradiation of solids, Phys. Rev. Lett. **85**, 2945 (2000).

[6] V. Malka, J. Faure, S. Fritzler, M. Manclossi, A. Guemnie-Tafo, E. d'Humières, E. Lefebvre, and D. Batani, Production of energetic proton beams with lasers, Rev. Sci. Instrum. **77**, 03B302 (2006).

[7] J. Workman, M. Nantel, A. Maksimchuk, and D. Umstadter, Application of a picosecond soft x-ray source to time-resolved plasma dynamics, Appl. Phys. Lett. **70**, 312 (1997).

[8] S. Svanberg, Some applications of ultrashort laser pulses in biology and medicine, Meas. Sci. Technol. **12**, 1777 (2001).

[9] S. H. Glenzer, G. Gregori, R. W. Lee, F. J. Rogers, S. W. Pollaine, and O. L. Landen, Demonstration of spectrally resolved x-ray scattering in dense plasmas, Phys. Rev. Lett. **90**, 175002 (2003).

[10] S. H. Glenzer, G. Gregori, F. J. Rogers, D. H. Froula, S. W. Pollaine, R. S. Wallace, and O. L. Landen, X-ray scattering from solid density plasmas, Phys. Plasmas **10**, 2433 (2003).

[11] S. H. Glenzer, O. L. Landen, P. Neumayer, R. W. Lee, K. Widmann, S. W. Pollaine, R. J. Wallace, G. Gregori, A. Höll, T. Bornath *et al.*, Observations of plasmons in warm dense matter, Phys. Rev. Lett. **98**, 065002 (2007).

[12] S. H. Glenzer and R. Redmer, X-ray thomson scattering in high energy density plasmas, Rev. Mod. Phys. **81**, 1625 (2009).

[13] K. Falk, C. L. Fryer, E. J. Gamboa, C. W. Greeff, H. M. Johns, D. W. Schmidt, M. Šmíd, J. F. Benage, and D. S. Montgomery, X-ray thomson scattering measurement of temperature in warm dense carbon, Plasma Phys. Control. Fusion **59**, 014050 (2017).

[14] H.-S. Park, D. M. Chambers, H.-K. Chung, R. J. Clarke, R. Eagleton, E. Giraldez, T. Goldsack, R. Heathcote, N. Izumi, M. H. Key *et al.*, High-energy Kα radiography using high-intensity, short-pulse lasers, Phys. Plasmas **13**, 056309 (2006).

[15] H.-S. Park, B. R. Maddox, E. Giraldez, S. P. Hatchett, L. T. Hudson, N. Izumi, M. H. Key, S. Le Pape, A. J. MacKinnon, A. G. MacPhee *et al.*, High-resolution 17–75kev backlighters for high energy density experiments, Phys. Plasmas **15**, 072705 (2008).

[16] W. L. Kruer, *The Physics Of Laser Plasma Interactions* (Addison-Wesley Publishing, California, 1988).

[17] Z. Zhang, M. Nishikino, H. Nishimura, T. Kawachi, A. S. Pirozhkov, A. Sagisaka, S. Orimo, K. Ogura, A. Yogo, Y. Okano *et al.*, Efficient multi-kev x-ray generation from a high-Z target irradiated with a clean ultra-short laser pulse, Opt. Express **19**, 4560 (2011).

[18] L. C. Jarrott, A. J. Kemp, L. Divol, D. Mariscal, B. Westover, C. McGuffey, F. N. Beg, M. Suggit, C. Chen, D. Hey *et al.*, Kα and bremsstrahlung x-ray radiation backlighter sources from short pulse laser driven silver targets as a function of laser pre-pulse energy, Phys. Plasmas **21**, 031211 (2014).

[19] T. Nishikawa, S. Suzuki, Y. Watanabe, O. Zhou, and H. Nakano, Efficient water-window x-ray pulse generation from femtosecond-laser-produced plasma by using a carbon nanotube target, Appl. Phys. B: Lasers Opt **78**, 885 (2004).

[20] S. Jiang, A. G. Krygier, D. W. Schumacher, K. U. Akli, and R. R. Freeman, Enhancing bremsstrahlung production from ultraintense laser-solid interactions with front surface structures, Eur. Phys. J. D **68**, 283 (2014).

[21] S. Gordon, R. Sheppard, T. Donnelly, D. Price, B. White, A. Osterheld, H. Hamster, A. Sullivan, and R. W. Falcone, X-ray emission from structured targets, in *Quantum Electronics and Laser Science Conference* (Optica Publishing Group, Baltimore, Maryland, 1993), p. QTuF2.

[22] S. P. Gordon, T. Donnelly, A. Sullivan, H. Hamster, and R. W. Falcone, X-rays from microstructured targets heated by femtosecond lasers, Opt. Lett. **19**, 484 (1994).

[23] G. Kulcsár, D. AlMawlawi, F. W. Budnik, P. R. Herman, M. Moskovits, L. Zhao, and R. S. Marjoribanks, Intense picosecond x-ray pulses from laser plasmas by use of nanostructured "velvet" targets, Phys. Rev. Lett. **84**, 5149 (2000).

[24] S. Mondal, I. Chakraborty, S. Ahmad, D. Carvalho, P. Singh, A. D. Lad, V. Narayanan, P. Ayyub, G. R. Kumar, J. Zheng, and Z. M. Sheng, Highly enhanced hard x-ray emission from oriented metal nanorod arrays excited by intense femtosecond laser pulses, Phys. Rev. B **83**, 035408 (2011).

[25] A. Ovchinnikov, O. Kostenko, O. Chefonov, O. Rosmej, N. Andreev, M. Agranat, J. Duan, J. Liu, and V. Fortov, Characteristic x-rays generation under the action of femtosecond laser pulses on nano-structured targets, Laser Part. Beams **29**, 249 (2011).

[26] Z. Samsonova, S. Höfer, T. Kämpfer, I. Uschmann, R. Röder, L. Trefflich, O. Rosmej, E. Förster, C. Ronning, D. Kartashov *et al.*, Hard x-ray generation from ZnO nanowire targets in a non-relativistic regime of laser-solid interactions, Appl. Sci. **8**, 1728 (2018).

[27] M. M. Mumane, H. C. Kapteyn, and R. W. Falcone, Structured targets for enhanced absorption and x-ray emission in femtosecond laser-produced plasmas, in *Optical Society of America Annual Meeting* (Optica Publishing Group, Boston, Massachusetts, 1990) p. MMM7.

[28] S. Kahaly, S. K. Yadav, W. M. Wang, S. Sengupta, Z. M. Sheng, A. Das, P. K. Kaw, and G. R. Kumar, Near-complete absorption of intense, ultrashort laser light by sub-λ gratings, Phys. Rev. Lett. **101**, 145001 (2008).

[29] W. Shang, J. Yang, W. Zhang, Z. Li, B. Deng, Y. Dong, T. Zhu, C. Huang, X. Zhan, Y. Mei *et al.*, Experimental demonstration of laser to x-ray conversion enhancements with low density gold targets, Appl. Phys. Lett. **108**, 064102 (2016).

[30] T. Ebert, N. W. Neumann, L. N. K. Döhl, J. Jarrett, C. Baird, R. Heathcote, M. Hesse, A. Hughes, P. McKenna, D. Neely *et al.*, Enhanced brightness of a laser-driven x-ray and particle source by microstructured surfaces of silicon targets, Phys. Plasmas **27**, 043106 (2020).

[31] F. Brunel, Not-so-resonant, resonant absorption, Phys. Rev. Lett. **59**, 52 (1987).

[32] A. L. Kritcher, P. Neumayer, H. J. Lee, T. Döppner, R. W. Falcone, S. H. Glenzer, and E. C. Morse, Demonstration of x-ray thomson scattering using picosecond Kα x-ray sources in the characterization of dense heated matter, Rev. Sci. Instrum. **79**, 10E739 (2008).

[33] P. Gibbon and E. Förster, Short-pulse laser-plasma interactions, Plasma Phys. Control. Fusion **38**, 769 (1996).

[34] P. Gibbon, *Short Pulse Laser Interactions with Matter: An Introduction* (Imperial College Press, London, 2005).

[35] S. Wilks and W. Kruer, Absorption of ultrashort, ultra-intense laser light by solids and overdense plasmas, IEEE J. Quantum Electron. **33**, 1954 (1997).

[36] H. Sawada, Y. Sentoku, T. Yabuuchi, U. Zastrau, E. Förster, F. N. Beg, H. Chen, A. J. Kemp, H. S. McLean, P. K. Patel, and Y. Ping, Monochromatic 2D Kα emission images revealing short-pulse laser isochoric heating mechanism, Phys. Rev. Lett. **122**, 155002 (2019).

[37] L. G. Huang, T. Kluge, and T. E. Cowan, Dynamics of bulk electron heating and ionization in solid density plasmas driven by ultra-short relativistic laser pulses, Phys. Plasmas **23**, 063112 (2016).

[38] M. N. Quinn, X. H. Yuan, X. X. Lin, D. C. Carroll, O. Tresca, R. J. Gray, M. Coury, C. Li, Y. T. Li, C. M. Brenner *et al.*,

Refluxing of fast electrons in solid targets irradiated by intense, picosecond laser pulses, Plasma Phys. Control. Fusion **53**, 025007 (2011).

[39] L. G. Huang, M. Molodtsova, A. Ferrari, A. L. Garcia, T. Toncian, and T. E. Cowan, Dynamics of hot refluxing electrons in ultra-short relativistic laser foil interactions, Phys. Plasmas **29**, 023102 (2022).

[40] L. J. Bae, U. Zastrau, H.-K. Chung, A. C. Bernstein, M. S. Cho, G. M. Dyer, E. Galtier, Z.-H. He, P. A. Heimann, G. B. Kang *et al.*, Diagnosis of warm dense conditions in foil targets heated by intense femtosecond laser pulses using Kα imaging spectroscopy, Opt. Express **26**, 6294 (2018).

[41] H.-K. Chung, M. Chen, and R. Lee, Extension of atomic configuration sets of the non-LTE model in the application to the Kα diagnostics of hot dense matter, High Energy Density Phys. **3**, 57 (2007).

[42] S. B. Hansen, A. Y. Faenov, T. A. Pikuz, K. B. Fournier, R. Shepherd, H. Chen, K. Widmann, S. C. Wilks, Y. Ping, H. K. Chung *et al.*, Temperature determination using Kα spectra from M-shell Ti ions, Phys. Rev. E **72**, 036408 (2005).

[43] J. Abdallah Jr, R. Clark, A. Faenov, L. Karpinski, S. Pikuz, V. Romanova, M. Sadowski, M. Scholz, and A. Szydlowski, Electron beam effects on the spectroscopy of multiply charged ions in plasma focus experiments, J. Quant. Spectrosc. Radiat. Transfer **62**, 85 (1999).

[44] T. Kawamura, H. Nishimura, F. Koike, Y. Ochi, R. Matsui, W. Y. Miao, S. Okihara, S. Sakabe, I. Uschmann, E. Förster, and K. Mima, Population kinetics on Kα lines of partially ionized Cl atoms, Phys. Rev. E **66**, 016402 (2002).

[45] D. Duston and J. Davis, Line emission from hot, dense, aluminum plasmas, Phys. Rev. A **21**, 1664 (1980).

[46] V. Bagnoud, B. Aurand, A. Blazevic, S. Borneis, C. Bruske, B. Ecker, U. Eisenbarth, J. Fils, A. Frank, E. Gaul *et al.*, Commissioning and early experiments of the phelix facility, Appl. Phys. B **100**, 137 (2010).

[47] F. Wagner, C. P. João, and J. Fils, Temporal contrast control at the phelix petawatt laser facility by means of tunable subpicosecond optical parametric amplification, Appl. Phys. B **116**, 429 (2014).

[48] F. Wagner, S. Bedacht, A. Ortner, M. Roth, A. Tauschwitz, B. Zielbauer, and V. Bagnoud, Pre-plasma formation in experiments using petawatt lasers, Opt. Express **22**, 29505 (2014).

[49] H. Legall, H. Stiel, V. Arkadiev, and A. Bjeoumikhov, High spectral resolution x-ray optics with highly oriented pyrolytic graphite, Opt. Express **14**, 4570 (2006).

[50] H. Legall, H. Stiel, M. Schnürer, M. Pagels, B. Kanngießer, M. Müller, B. Beckhoff, I. Grigorieva, A. Antonov, V. Arkadiev, and A. Bjeoumikhov, An efficient x-ray spectrometer based on thin mosaic crystal films and its application in various fields of x-ray spectroscopy, J. Appl. Crystallogr. **42**, 572 (2009).

[51] T. Ebert, R. Heber, T. Abel, J. Bieker, G. Schaumann, and M. Roth, Targets with cone-shaped microstructures from various materials for enhanced high-intensity laser–matter interaction, High Power Laser Sci. Eng. **9**, e24 (2021).

[52] B. R. Maddox, H. S. Park, B. A. Remington, N. Izumi, S. Chen, C. Chen, G. Kimminau, Z. Ali, M. J. Haugh, and Q. Ma, High-energy x-ray backlighter spectrum measurements using calibrated image plates, Rev. Sci. Instrum. **82**, 023111 (2011).

[53] H.-K. Chung, M. Chen, W. Morgan, Y. Ralchenko, and R. Lee, FLYCHK: Generalized population kinetics and spectral model for rapid spectroscopic analysis for all elements, High Energy Density Phys. **1**, 3 (2005).

[54] B. Westover, A. MacPhee, C. Chen, D. Hey, T. Ma, B. Maddox, H.-S. Park, B. Remington, and F. N. Beg, Study of silver Kα and bremsstrahlung radiation from short-pulse laser-matter interactions with applications for x-ray radiography, Phys. Plasmas **17**, 082703 (2010).

[55] Y. Sentoku and A. Kemp, Numerical methods for particle simulations at extreme densities and temperatures: Weighted particles, relativistic collisions and reduced currents, J. Comput. Phys. **227**, 6846 (2008).

[56] T. Ebert, Enhancing laser-induced x-ray emission and ion acceleration with microstructured targets, Ph.D. thesis, Technische Universität Darmstadt, 2021.

[57] H. Chen, R. Shepherd, H. K. Chung, A. Kemp, S. B. Hansen, S. C. Wilks, Y. Ping, K. Widmann, K. B. Fournier, G. Dyer *et al.*, Fast-electron-relaxation measurement for laser-solid interaction at relativistic laser intensities, Phys. Rev. E **76**, 056402 (2007).

[58] E. Eftekhari-Zadeh, M. S. Blümcke, Z. Samsonova, R. Loetzsch, I. Uschmann, M. Zapf, C. Ronning, O. N. Rosmej, D. Kartashov, and C. Spielmann, Laser energy absorption and x-ray generation in nanowire arrays irradiated by relativistically intense ultra-high contrast femtosecond laser pulses, Phys. Plasmas **29**, 013301 (2022).

[59] J. A. Cobble, S. Palaniyappan, R. P. Johnson, T. Shimada, C. Huang, D. C. Gautier, D. D. Clark, K. Falk, and D. Jung, Laser-driven micro-Coulomb charge movement and energy conversion to relativistic electrons, Phys. Plasmas **23**, 093113 (2016).

[60] A. Alejo, D. Gwynne, D. Doria, H. Ahmed, D. Carroll, R. Clarke, D. Neely, G. Scott, M. Borghesi, and S. Kar, Recent developments in the thomson parabola spectrometer diagnostic for laser-driven multi-species ion sources, J. Instrum. **11** (10), C10005 (2016).

[61] A. Laso Garcia, A. Hannasch, M. Molodtsova, A. Ferrari, J. P. Couperus Cadabağ, M. C. Downer, A. Irman, S. D. Kraft, J. Metzkes-Ng, L. Naumann, I. Prencipe, U. Schramm, K. Zeil, R. Zgadzaj, T. Ziegler, and T. E. Cowan, Calorimeter with Bayesian unfolding of spectra of high-flux broadband x rays, Rev. Sci. Instrum. **93**, 043102 (2022).

[62] H. Habara, K. Ohta, K. A. Tanaka, G. R. Kumar, M. Krishnamurthy, S. Kahaly, S. Mondal, M. K. Bhuyan, R. Rajeev, and J. Zheng, Direct, absolute, and *in situ* measurement of fast electron transport via cherenkov emission, Phys. Rev. Lett. **104**, 055001 (2010).

[63] M. F. Gu, The flexible atomic code, Can. J. Phys. **86**, 675 (2008).

[64] K. U. Akli, S. B. Hansen, A. J. Kemp, R. R. Freeman, F. N. Beg, D. C. Clark, S. D. Chen, D. Hey, S. P. Hatchett, K. Highbarger *et al.*, Laser heating of solid matter by light-pressure-driven shocks at ultrarelativistic intensities, Phys. Rev. Lett. **100**, 165002 (2008).

[65] N. F. Beier, H. Allison, P. Efthimion, K. A. Flippo, L. Gao, S. B. Hansen, K. Hill, R. Hollinger, M. Logantha, Y. Musthafa *et al.*, Homogeneous, micron-scale high-energy-density matter

generated by relativistic laser-solid interactions, Phys. Rev. Lett. **129**, 135001 (2022).

[66] X. Llovet, C. J. Powell, F. Salvat, and A. Jablonski, Cross sections for inner-shell ionization by electron impact, J. Phys. Chem. Ref. Data **43**, 013102 (2014).

[67] S. Sander, T. Ebert, D. Hartnagel, M. Hesse, X. Pan, G. Schaumann, M. Šmíd, K. Falk, and M. Roth, Microstructured layered targets for improved laser-induced x-ray backlighters, Phys. Rev. E **104**, 065207 (2021).